Inorganic Chemistry

Article

pubs.acs.org/IC

Exploring the Noninnocent Character of Electron Rich π-Extended 8-Oxyquinolate Ligands in Ruthenium(II) Bipyridyl Complexes

Stephanie Bellinger-Buckley,[†] Tse-Cing Chang,[‡] Seema Bag,[†] David Schweinfurth,[§] Weihong Zhou,[†] Bela Torok,[†] Biprajit Sarkar,[§] Ming-Kang Tsai,*[,‡] and Jonathan Rochford*[,†]

[†]Department of Chemistry, University of Massachusetts—Boston, 100 Morrissey Boulevard, Boston, Massachusetts 02125, United States

[‡]Department of Chemistry, National Taiwan Normal University, Number 88, Section 4, Ting-Chow Road, Taipei, 11677 Taiwan ROC

[§]Institut für Chemie und Biochemie, Anorganische Chemie, Freie Universität Berlin, Fabeckstrasse 34-36, Berlin, Germany

Supporting Information

ABSTRACT: A series of ruthenium polypyridyl complexes are presented incorporating π-extended electron rich derivatives of the 8-oxyquinolate (OQN) ligand. The π-donating property of the OQN ligand introduces covalent character to the Ru(dπ)−OQN(π) bonding scheme enhancing its light harvesting properties and diversifying its redox properties, relative to the classic ruthenium(II) trisbipyridyl complex $[Ru(bpy)_3]^{2+}$. Synthesis and characterization is presented for the complexes $[Ru(bpy)_2(R\text{-}OQN)](PF_6)$, where bpy = 2,2′-bipyridine and R = 5-phenyl, 5,7-diphenyl, 2,4-diphenyl, 5,7-bis(4-methoxyphenyl), 5,7-bis(4-(diphenylamino)phenyl). A comprehensive bonding analysis is presented for the $[Ru(bpy)_2(OQN)]^+$ system illustrating the origin of its unique spectroscopic and redox properties relative to $[Ru(bpy)_3]^{2+}$. This model is then extended to enable a consistent interpretation of spectra and redox properties for the π-extended $[Ru(bpy)_2(R\text{-}OQN)](PF_6)$ series. Electronic structures have been probed experimentally by a combination of electrochemical and spectroscopic techniques (UV−vis−NIR absorption, emission, EPR spectroscopy) where (metal−ligand)-to-ligand (MLLCT) charge-transfer properties are described by time dependent-density functional theory (TD-DFT) analysis, at the B3LYP/6-31g(d,p) level of approximation. Substantial mixing, due to bonding and antibonding combinations of Ru(dπ) and OQN(π) orbitals, is observed at the HOMO and HOMO − 3 levels for the ruthenium−oxyanion bond in $[Ru(bpy)_2(OQN)]^+$, which is responsible for the low-energy MLLCT based electronic transition and destabilization of the HOMO level viz. cyclic voltammetry. This noninnocent π-bonding phenomenon is consistent throughout the series which allows for controlled tuning of complex redox potentials while maintaining panchromatic absorption properties across the visible spectrum. Extensive charge delocalization is observed for the one-electron oxidized species using a combination of UV−vis−NIR, EPR spectroelectrochemistry, and Mulliken spin-density analysis, giving strong evidence for hole-delocalization across the delocalized Ru(dπ)−OQN(π) system, in particular for the electron rich 5,7-bis(4-methoxyphenyl) and 5,7-bis(4-(diphenylamino)phenyl) systems.

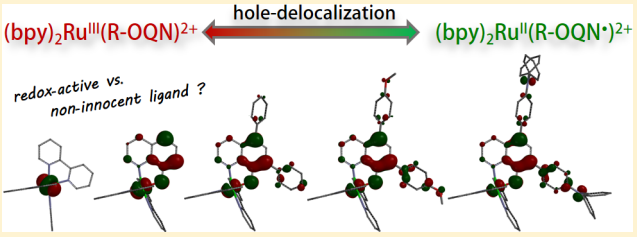

INTRODUCTION

Ruthenium polypyridyl complexes are very well-established as highly diverse photochemical and redox systems due to their strong visible absorption, long excited state lifetimes, redox stability, and efficient electron transfer properties. Studies have ranged from purely dark redox chemistry taking advantage of their electron/hole mediating and catalytic properties,[1−7] light-harvesting of diffuse solar radiation,[8−11] and multiphoton nonlinear photonics.[12−14] The unique photophysical properties of $[Ru(bpy)_3]^{2+}$ are characterized by its strong ^{1}MLCT visible absorption (λ_{max} = 454 nm, ε = 14 600 M^{-1} cm^{-1}), metastable ^{3}MLCT excited state ($\tau \sim 1$ μs), and reversible redox chemistry (E° = 1.29 V vs SCE).[15−17] These attractive properties of ruthenium(II) polypyridyl systems stem from the localized ruthenium dπ and polypyridyl π* orbitals, each of which show independent redox active behavior, i.e., Ru(III/II) and bpy(0/•−) redox states.[18−21] Recently there has been a renewed and expanding interest in redox active transition metal systems which incorporate metal−ligand π-bonding, or so-called "noninnocent" ligands.[22−34] The term "noninnocent ligand" implies that the ligand in question forms hybrid metal(dπ)−ligand(π) molecular orbitals which preclude formal assignment of the central metal oxidation state.[27,34] Such a bonding scenario opens the opportunity to explore diverse electronic distributions in π-conjugated metal−ligand frameworks where the photophysical and redox properties may be tailored by design, in particular for photovoltaic applica-

Received: February 2, 2014
Published: May 19, 2014

   dx.doi.org/10.1021/ic5002623 | Inorg. Chem. 2014, 53, 5556−5567

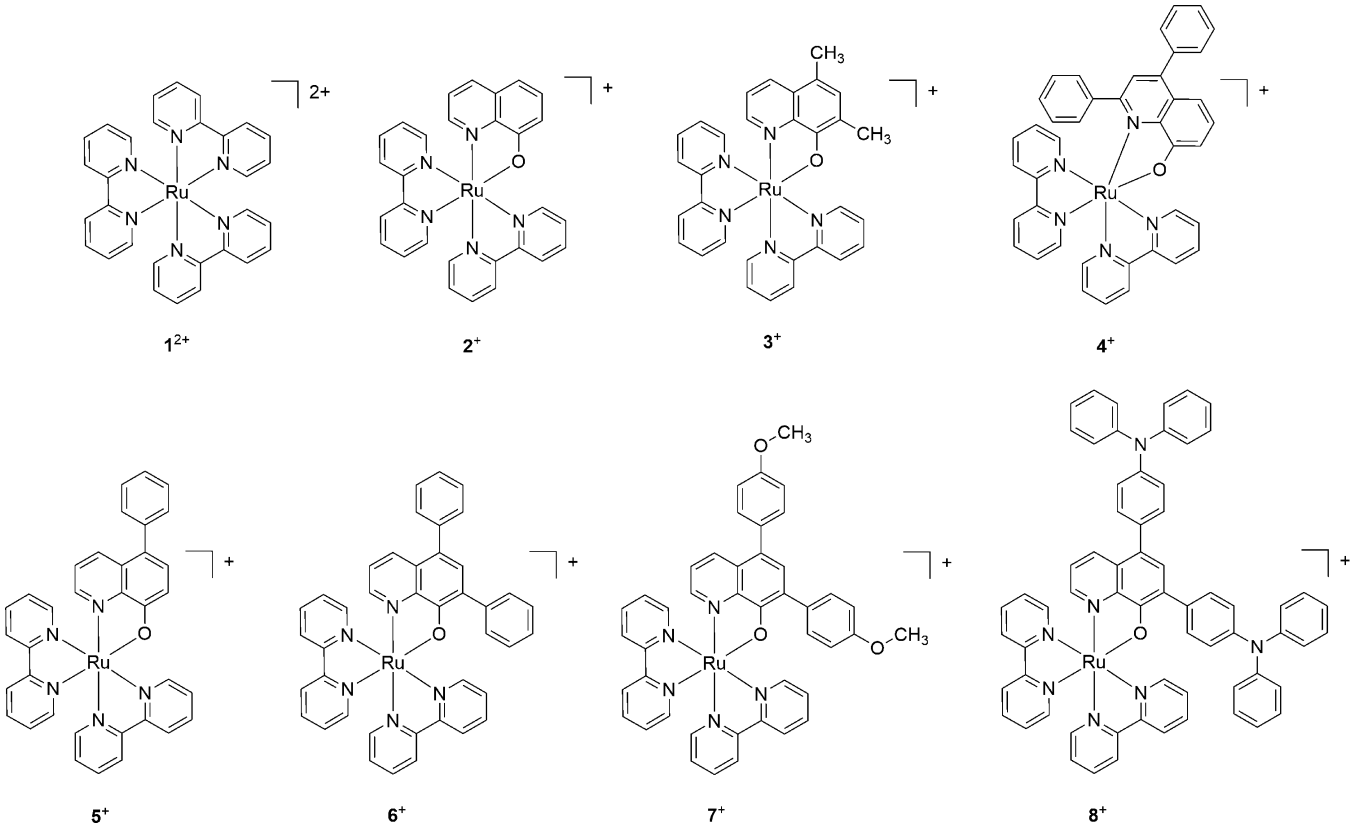

Figure 1. Structures of $[Ru(bpy)_2(R\text{-}OQN)]^+$ complexes $\mathbf{2}^+$–$\mathbf{8}^+$ investigated here including the $[Ru(bpy)_3]^{2+}$ reference complex $\mathbf{1}^{2+}$.

Scheme 1. (a) Synthetic Procedure Employed in the Synthesis of the 2,4-Diphenyl-8-hydroxyquinoline [*i*-Ph_2OQN(H)] Ligand, (b) Suzuki Coupling Conditions Employed in the Synthesis of the 5,7-Bisaryl-8-hydroxyquinoline Ligands, and (c) Synthesis of the $Ru(bpy)_2(R\text{-}OQN)]^+$ Complexes

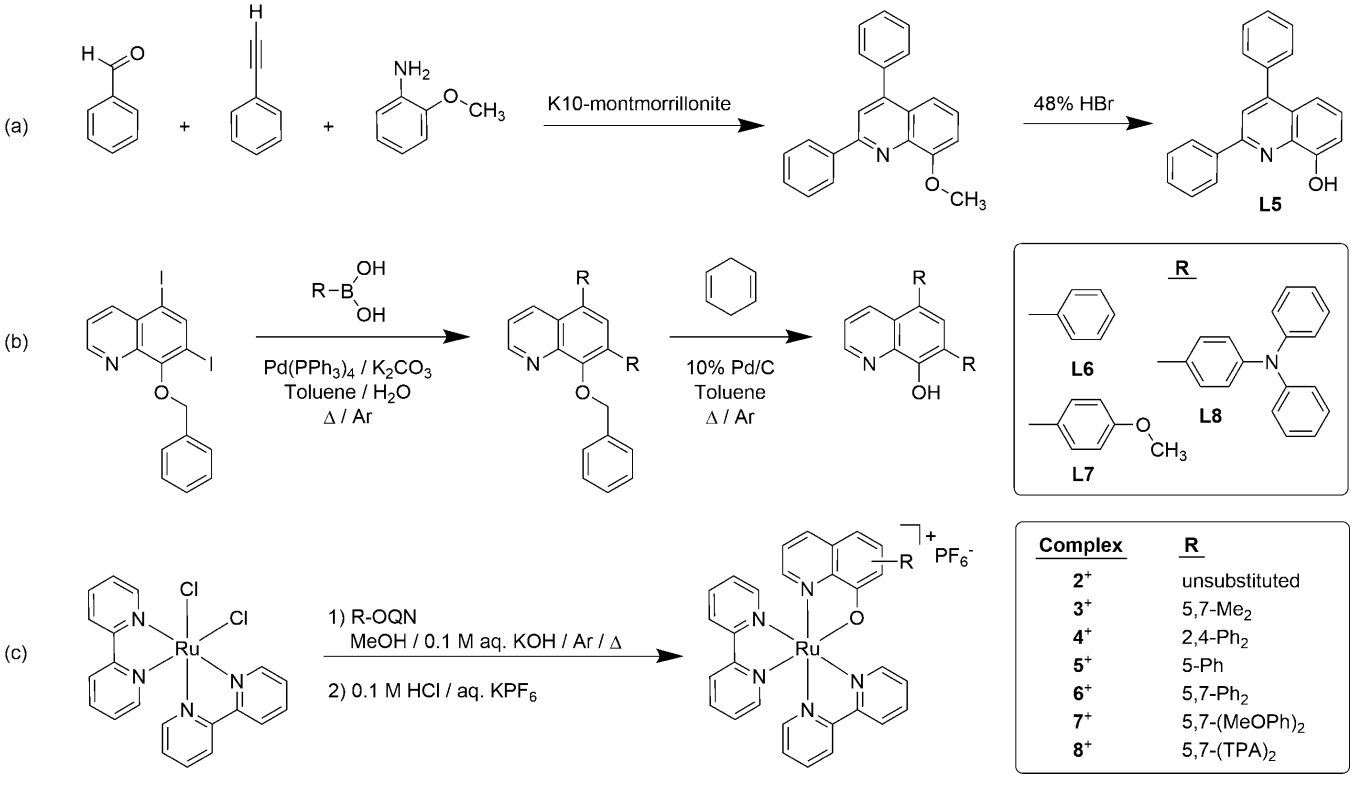

Complex	R
$\mathbf{2}^+$	unsubstituted
$\mathbf{3}^+$	5,7-Me_2
$\mathbf{4}^+$	2,4-Ph_2
$\mathbf{5}^+$	5-Ph
$\mathbf{6}^+$	5,7-Ph_2
$\mathbf{7}^+$	5,7-$(MeOPh)_2$
$\mathbf{8}^+$	5,7-$(TPA)_2$

dx.doi.org/10.1021/ic5002623 | *Inorg. Chem.* 2014, 53, 5556–5567

tions.[35,36] This body of work aims to investigate the noninnocent character of the 8-oxyquinolate (OQN) ligand at the d^6 ruthenium center and, in addition, to explore the influence of π-extension and peripheral redox active groups on its electronic properties. There remain limited reports of Ru−OQN systems in the literature[35,37−44] with most recent studies demonstrating their application as a photosensitizer in TiO_2 based solar cells and even as water oxidation catalysts using the tridentate 2-carboxy-8-oxyquinolate ligand at a ruthenium(II) aqua center.[35,43] To develop a greater understanding of the electronic structure of the Ru(dπ)−OQN(π) system toward application in photoelectrochemical and electrocatalytic systems a series of $[Ru(bpy)_2(R\text{-}OQN)](PF_6)$ complexes, where bpy = 2,2′-bipyridine and R = 5-phenyl, 5,7-diphenyl, 2,4-diphenyl, 5,7-bis(4-methoxyphenyl), 5,7-bis(4-(diphenylamino)phenyl), hereafter referred to as TPA_2OQN, have been designed to explore the impact of π-delocalization and electron-donation on their photophysical and redox properties (Figure 1).

RESULTS AND DISCUSSION

Synthesis. The unsubstituted 8-hydroxyquinoline and 5,7-dimethyl-8-hydroxyquinoline ligands are commercially available whereas their 5,7-substituted derivatives with π-extended functional groups are less common. Fortunately there has been some interest in the development of π-extended 8-hydroxyquinoline ligands in recent years due to its significance in the tailoring of organoboron based light-emitting diode devices. In particular the combined works of Hormi, Anzenbacher, and Jaekle have independently demonstrated the influence of alkenyl, ethynyl, and aryl substitution at the 2, 4, 5, and 7 positions of the OQN ligand when bound to redox inert boron, aluminum, or zinc centers.[45−51] In this study we have adapted standard Suzuki coupling conditions for the introduction of the aryl substitutents phenyl, 4-methoxyphenyl, and 4-(diphenylamino)phenyl groups at 5,7-positions of the OQN ligand using the appropriate boronic acids (Scheme 1). The monosubstituted 5-phenyl-8-hydroxyquinoline ligand was prepared according to a literature method where the 5-chloro position of the tosylate protected 5-chloro-8-oxyquinoline reagent is selectively activated to Suzuki coupling by virtue of the *para* electron withdrawing tosyl substitutent, often itself active under Suzuki conditions.[47] Key to success of 5,7-substitution is the benzyl protected 5,7-diodo-8-oxyquinoline intermediate where the benzyl group plays a dual role in passivating the ligand chelation properties and aiding its solubility, thus facilitating optimum reactivity. This step is followed by reductive cleavage of the benzyl protecting group using cyclohexadiene as a hydrogen source in the presence of a Pd/C catalyst to generate the neutral 8-hydroxyquinoline ligand precursor.[52] The 2,4-diphenyl-8-hydroxyquinoline ligand was prepared following a convenient one-pot microwave synthesis to allow comparison of OQN π-extension at either the pyridyl or phenoxy side of the ligand.[53] Once isolated, the 8-hydroxyquinoline ligand precursors underwent a straightforward complexation at the ruthenium(II) bis(2,2-bipydidyl) core using a mixture of methanol and aqueous potassium hydroxide. Analytically pure $[Ru(bpy)_2(R\text{-}OQN)](PF_6)$ salts were isolated via KPF_6 mediated metathesis resulting in analytically pure dark reddish-brown solids.

Computational Analysis. As an aid for the assignment of electronic transitions and redox transformations presented below for the $[Ru(bpy)_2(R\text{-}OQN)]^+$ series of complexes, a prior theoretical analysis of their frontier orbitals is warranted. Introduction of the π-donating OQN ligand at the Ru(II) center dramatically alters the classical D_3 σ-bonding scenario of $[Ru(bpy)_3]^{2+}$ (hereafter denoted as $\mathbf{1}^{2+}$),[20,21] as the reduced C_1 symmetry of $[Ru(bpy)_2(OQN)]^+$ causes a breakdown of degeneracy in its electronic structure and destabilizes the HOMO level (Supporting Information Figure SI-1). Of particular note is the Ru(dπ)−OQN(π) interaction which is responsible for a bonding/antibonding pair of occupied molecular orbitals, HOMO − 3 and HOMO, respectively (Figure 2). These energy levels are of significant interest to this

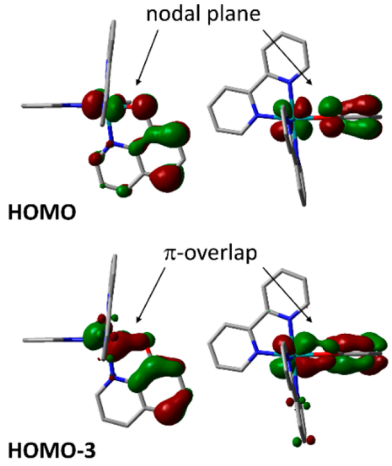

Figure 2. Aerial and side-on perspective views of both the HOMO and HOMO − 3 levels for $\mathbf{2}^+$ illustrating the π-bonding/antibonding combination of Ru(dπ) and OQN(π) systems. For complete DFT results please refer to the Supporting Information. An acetonitrile polarizable continuum model was employed using the B3LYP functional and 6-31g(d,p) (C,H,N,O) and LANL08 (Ru) basis sets.

study due to their noninnocent character derived from covalent mixing of both the central metal dπ and ligand π manifolds.

A summary of metal−ligand percentage contributions to the HOMO orbital for complexes $\mathbf{1}^{2+}$−$\mathbf{8}^+$ is presented in Table 1 alongside their calculated energies. In contrast to the localized $\mathbf{1}^{2+}$ system, the HOMO level of complexes $\mathbf{2}^+$−$\mathbf{8}^+$ is dominated by >60% contribution from the R-OQN ligands where an increasing influence is evident for electron-donating substitutents with the triphenylamine and OQN components contributing equally to 88% of the HOMO for complex $\mathbf{8}^+$.

Beyond the HOMO energy level, the HOMO − 1 and HOMO − 2 levels are dominated by the ruthenium center for $\mathbf{2}^+$−$\mathbf{7}^+$ with further contribution from the R-OQN ligands found at lower energies. In contrast, for complex $\mathbf{8}^+$ the electron rich triphenylamine substituents dominate the HOMO − 1 and HOMO − 2 levels with subsequent ruthenium centered orbitals found at lower energy. This is best illustrated by the frontier molecular orbital contribution plot presented in Figure 3 and is also relevant for interpretation of electrochemical data presented below. Comprehensive molecular orbital percent contribution plots are provided in the Supporting Information for all complexes $\mathbf{1}^{2+}$−$\mathbf{8}^+$.

To summarize the frontier orbital energies for all complexes $\mathbf{1}^{2+}$−$\mathbf{8}^+$ a molecular orbital energy diagram is presented in Figure 4. Consistent with the UV−vis absorption data and electrochemical data presented below, a larger HOMO−LUMO band gap of 3.48 eV is observed for $\mathbf{1}^{2+}$ with the R-OQN series displaying a narrower band gap ranging from 2.52

dx.doi.org/10.1021/ic5002623 | Inorg. Chem. 2014, 53, 5556−5567

Table 1. Metal−Ligand Contributions (%) to the HOMO of Complexes 1^{2+}−8^{+} As Determined by DFT Analysis Including Calculated HOMO Energies[a]

	Ru d(π)	OQN(π)	R	bpy (total)	energy (eV)
1^{2+} $[Ru(bpy)_3]^{2+}$	85	0		15	−6.07
2^{+} $[Ru(bpy)_2(OQN)]^{+}$	32	63		5	−4.99
3^{+} $[Ru(bpy)_2(Me_2OQN)]^{+}$	22	75		3	−4.81
4^{+} $[Ru(bpy)_2(i\text{-}Ph_2OQN)]^{+}$	31	64	1 (i-Ph_2)	4	−4.92
5^{+} $[Ru(bpy)_2(PhOQN)]^{+}$	25	65	6 (Ph)	4	−4.94
6^{+} $[Ru(bpy)_2(Ph_2OQN)]^{+}$	24	60	12 (Ph_2OQN)	4	−4.90
7^{+} $\{Ru(bpy)_2[(MeOPh)_2OQN]\}^{+}$	16	61	20 $(MeOPh)_2$	3	−4.78
8^{+} $[Ru(bpy)_2(TPA_2OQN)]^{+}$	10	45	43 (TPA_2)	2	−4.70

[a]R illustrates the increasing contribution from π-conjugated substituents at the OQN ligand when ascending the series. An acetonitrile polarizable continuum model was employed using the B3LYP functional and 6-31g(d,p) (C,H,N,O) and LANL08 (Ru) basis sets.

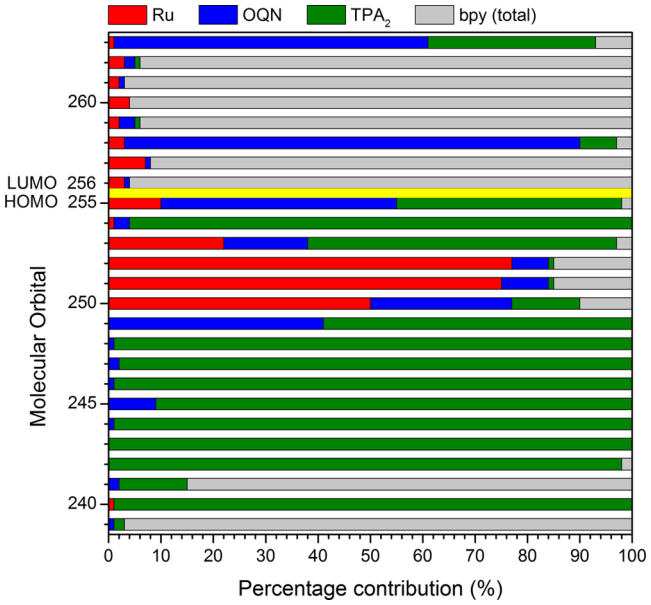

Figure 3. Percentage contributions of Ru, OQN, TPA, and bpy fragments to select frontier molecular orbitals of 8^{+}. Filled and valence levels are separated by a yellow row between the HOMO (255) and LUMO (256) levels. An acetonitrile polarizable continuum model was employed using the B3LYP functional and 6-31g(d,p) (C,H,N,O) and LANL08 (Ru) basis sets.

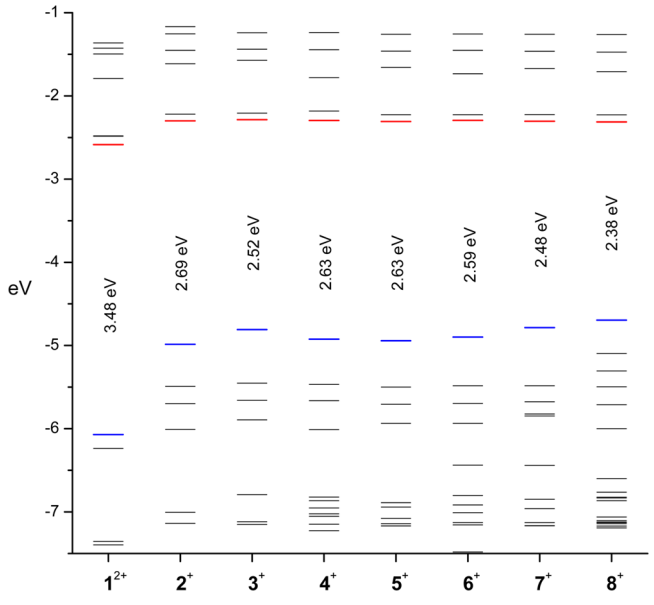

Figure 4. Plot of molecular orbital energy levels (eV) for complexes 1^{2+}−8^{+} as calculated by DFT/B3LYP/6-31g(d,p) (C,H,N,O) and LANL08 (Ru) in an acetonitrile solvent continuum model. Electron occupancy is removed for clarity, and HOMO and LUMO levels are highlighted in blue and red, respectively.

to 2.89 eV depending upon the nature of the OQN ring substituents. In contrast to the delocalized HOMO orbital, the LUMO level remains bpy(π*) based for all complexes.

UV−Vis Electronic Absorption Spectra and TDDFT. The $[Ru(bpy)_2(R\text{-}OQN)]^{+}$ complexes 2^{+}−8^{+} have a dark reddish-brown appearance in contrast to the bright orange color of 1^{2+}. As discussed in the computational analysis above, introduction of the π-donating R-OQN ligand is responsible for a significant reduction in HOMO−LUMO band gap for these complexes with an associated breaking of degeneracy. A similar destabilization of the HOMO level has been previously reported for a series of isostructural ruthenium sulfoxide complexes.[54] All oxyquinolate complexes display analogous absorption bands in the visible region with comparable maxima and extinction coefficients. The UV−vis spectra for select complexes are shown in Figure 5 with the complete set of spectra for complexes 1^{2+}−8^{+} available in the Supporting Information (Figure SI-2). The low energy maximum absorption observed for 2^{+} at 496 nm (ε = 12 100 M^{-1} cm^{-1}) undergoes a slight bathochromic shift of 10−15 nm

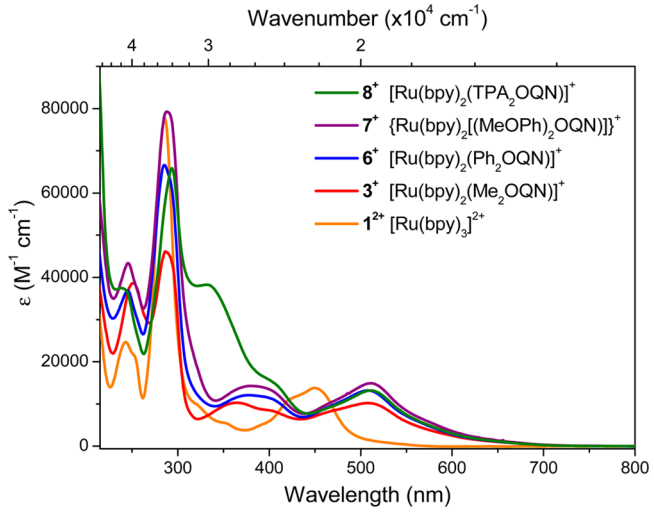

Figure 5. Overlay of UV−vis electronic absorption spectra of select complexes (for clarity) recorded in acetonitrile.

dx.doi.org/10.1021/ic5002623 | Inorg. Chem. 2014, 53, 5556−5567

(398−592 cm^{-1}) with substitution either at the 2,4 (4^+), 5 (5^+), or 5,7 (3^+, 6^+, 7^+, 8^+) positions with the 5,7-bis(4-(diphenylamino)phenyl)OQN complex 8^+ showing the lowest energy maximum absorption at 511 nm (ε = 13 200 M^{-1} cm^{-1}).

The computed TD-DFT spectra including molecular orbital contributions and relevant molecular orbital images for 8^+ are shown in Figures 6 and 7 with the complete series of data included in the Supporting Information.

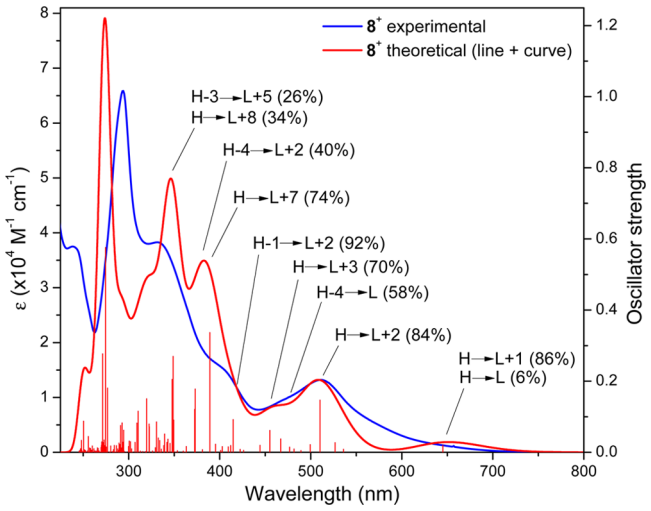

Figure 6. Overlay of experimental and theoretical TD-DFT spectra for 8^+ in acetonitrile. An acetonitrile polarizable continuum model was employed using the B3LYP functional and 6-31g(d,p) (C,H,N,O) and LANL08 (Ru) basis sets.

Most notable for all oxyquinolate substituted complexes is a splitting of the characteristic 450 nm ^{1}MLCT absorption band of 1^{2+} into higher and lower frequency absorptions of comparable intensity. The lowest energy absorption maximum is in fact due to numerous contributing electronic transitions including HOMO − 2 → LUMO and HOMO − 1 → LUMO + 1 with the greatest contribution to this absorption band, across the series 2^+−8^+, consistently from the HOMO → LUMO + 2 electronic transition. This excitation is unique to this class of complex in that it originates from the highest energy, filled and delocalized Ru(dπ)−OQN(π) HOMO level with the destination orbital for the transition being R-OQN(π^*) in nature. As such this absorption band is most accurately described as a singlet (metal−ligand)-to-ligand charge transfer (^{1}MLLCT) electronic transition. Consistent for all spectra is how the low energy absorption band gradually tails off beyond 700 nm due to additional underlying electronic transitions. These are assigned to the weak oscillator strength HOMO → LUMO + 1 and HOMO → LUMO transitions again originating from the same delocalized Ru(dπ)−OQN(π) orbital and are therefore also ^{1}MLLCT in character with lower energy bpy(π^*) destination orbitals. The higher energy visible absorption band occurring in the range 360−400 nm is more typical of traditional ruthenium polypyridyl systems being derived primarily from a localized Ru(dπ) → bpy(π^*) ^{1}MLCT transition. However, even here there exists significant contribution from [Ru(dπ)−OQN(π)] → R-OQN(π^*) electronic transitions involving higher energy R-OQN(π^*) orbitals, for example HOMO → LUMO + 7 in 8^+ (Figure 6). The strong enhancement of absorption for 8^+ in the UV region at 331 nm is assigned to a combination of [Ru(dπ)−OQN(π)] → bpy(π^*) (HOMO → LUMO + 5) and [Ru(dπ)−OQN(π)] → $(TPA)_2$OQN(π^*) (HOMO → LUMO + 7) ^{1}MLLCT transitions. A complete database comparing experimental and theoretical TD-DFT derived spectra, including assignments of all electronic transitions and electron density maps of contributing molecular orbitals, is provided in the Supporting Information for all complexes. A summary of spectral data for complexes 1^{2+}−8^+ recorded in acetonitrile is provided in Table 2.

In addition to its characteristic visible absorption properties, 1^{2+} has been widely studied for its phosphorescent properties

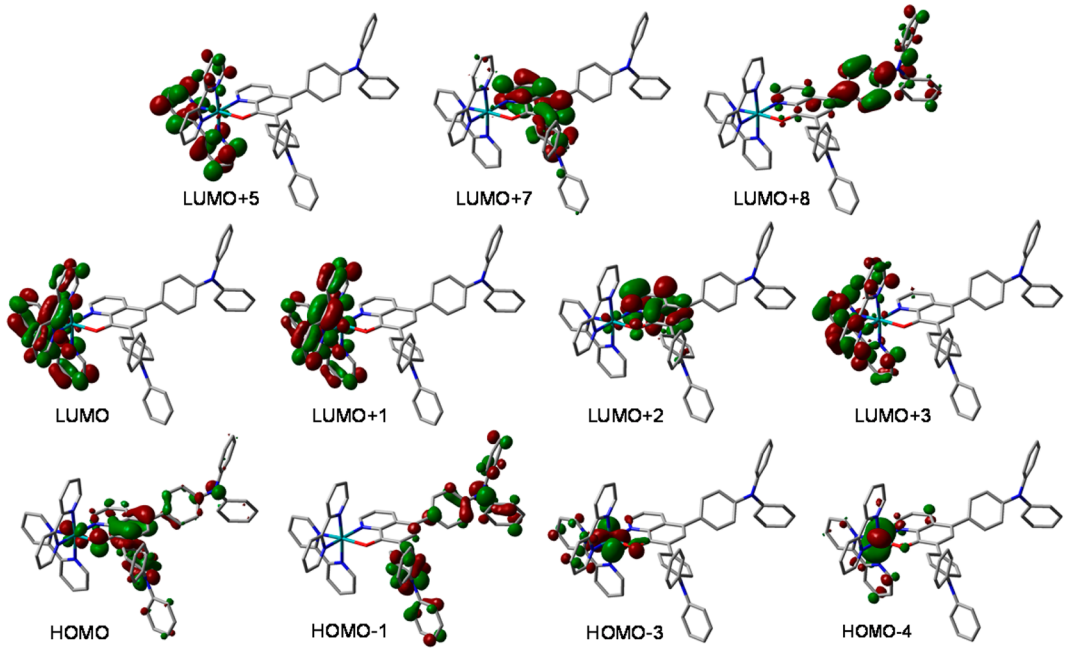

Figure 7. Select molecular orbitals for 8^+ determined responsible for the major UV−vis electronic transitions by TD-DFT analysis.

dx.doi.org/10.1021/ic5002623 | Inorg. Chem. 2014, 53, 5556−5567

Table 2. Electronic Absorption and Phosphorescence Emission Data for Complexes 1^{2+}–8^{+}

	absorption[a] λ_{max} (nm) ($\varepsilon \times 10^4$ M^{-1} cm^{-1})	emission λ_{max} (nm)[b]
1^{2+}	243 (2.49), 286 (7.79), 430 (sh), 450 (1.46)	581, 630, 680 (sh)
2^{+}	257 (4.20), 291 (4.31), 360 (0.90), 400 (0.77), 496 (1.21)	703, 761 (sh)
3^{+}	250 (3.86), 286 (4.61), 365 (1.30), 400 (sh), 507 (1.02)	724, 777 (sh)
4^{+}	251 (3.07), 272 (3.34), 295 (3.51), 370 (0.79), 405 (0.83), 506 (0.86)	730, 790 (sh)
5^{+}	246 (3.99), 256 (3.82), 293 (4.99), 369 (1.11), 398 (1.03), 505 (1.35)	702, 758 (sh)
6^{+}	245 (3.69), 285 (6.67), 377 (1.21), 508 (1.32)	704, 760 (sh)
7^{+}	246 (4.33), 288 (7.93), 382 (1.42), 510 (1.49)	712, 772 (sh)
8^{+}	238 (3.75), 294 (6.56), 331 (3.83), 390 (sh), 511 (1.32)	708, 766 (sh)

[a]Recorded at room temperature in acetonitrile. [b]Recorded at 77 K in an ethanol/methanol (4:1) frozen glass.

with an absolute quantum yield of Φ_{phos} = 0.095 reported in acetonitrile at room temperature.[55] The low temperature phosphorescence spectrum of 1^{2+} in an ethanol/methanol (4:1) 77 K frozen glass is illustrated in Supporting Information Figure SI-3 displaying three closely resolved ^{3}MLCT excited states with maxima at 581 and 630 and a shoulder at 680 nm ($\Delta\nu \sim 1340$ cm^{-1}).[56] In comparison, all oxyquinolate complexes 2^{+}–8^{+} show very weak emission only observable at reduced temperature. Emission maxima are all shifted by over 3000 cm^{-1} relative to 1^{2+} occurring in the range 702–730 nm for the series 2^{+}–8^{+}. Similar to 1^{2+}, fine structure is observed with a weaker shoulder peak present on the low energy side of the principle emission peak ($\Delta\nu \sim 1040$ cm^{-1}). Attempts to record accurate quantum yields were in vain due to the weak nature of the emission with no signal observed at room temperature. Furthermore, radiative decay constants were beyond the time resolution of our instrument (~200 ps) which is in accordance with the weak intensity of the steady state spectra. Invoking Kasha's rule, as confirmed by excitation spectra (Supporting Information Figures SI-4 to SI-10), and assuming efficient intersystem crossing typical of d^6 ruthenium polypyridyl complexes, it is likely that the poor photoluminescence response of these complexes is due to rapid ^{1}MLLCT → ^{3}MLLCT intersystem crossing followed by population of a metal centered ^{3}MC $(d\pi)^5(\sigma^*)^1$ electronic excited state which undergoes efficient nonradiative decay.[56−60] While such behavior is typical of ruthenium polypyridyl complexes, it is also possible that the ^{3}MC state in $[Ru(bpy)_2(R{-}OQN)]^{+}$ complexes actually has substantial ligand contribution via strong $d\pi$–$p\pi$ mixing. This would serve to increase the electron-vibrational coupling constant (S_M) and excited-state/ground-state vibrational overlap ultimately increasing the nonradiative rate constant (k_{nr}) consistent with our observations.[61]

Electrochemistry. Redox potentials for the series 1^{2+}–8^{2+} were recorded by cyclic voltammetry in an acetonitrile electrolyte, and the data are summarized in Table 3 in reference to SCE. A selection of cyclic voltammograms are also presented in Figure 8 to illustrate influence of the OQN ligand

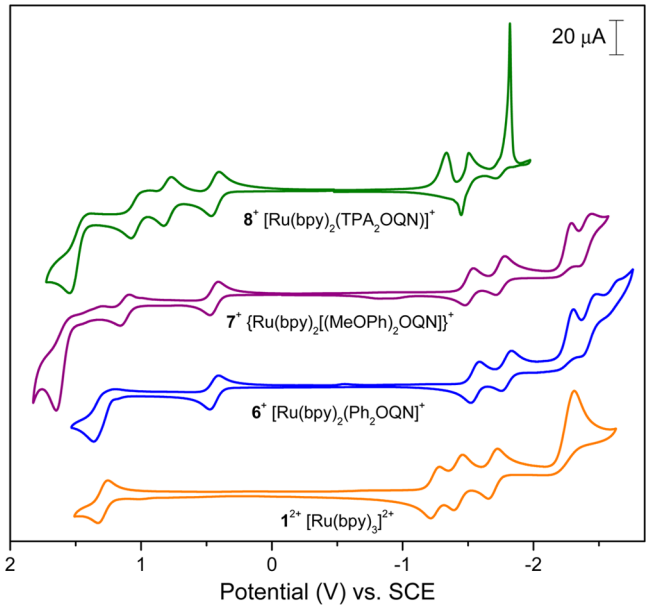

Figure 8. Overlay of cyclic voltammograms for 1^{2+} $[Ru(bpy)_3]^{2+}$, and the 5,7-substituted $[Ru(bpy)_2(R\text{-}OQN)]^{+}$ derivatives 6^{+}, 7^{+}, and 8^{+}, recorded in acetonitrile (0.1 M Bu_4NPF_6) at a glassy carbon working electrode with scan rate 50 mV s^{-1}.

on redox potentials at the Ru(II) bis(bipyridyl) core and to inform on the redox properties of the π-extended (6^{+}) and electron donating (7^{+}, 8^{+}) derivatives. All R-OQN complexes show reversible first oxidations within a potential range E° = +0.40 V to +0.52 V demonstrating a strong cathodic shift relative to 1^{2+} (E° = +1.29 V). This is unsurprising considering the introduction of an anionic ligand at the Ru(II) center; however, in agreement with the DFT electronic assignments, this first redox couple is assigned to oxidation–reduction of the delocalized $Ru(d\pi)$–$OQN(\pi)$ HOMO energy level, i.e., a $[Ru(OQN)]^{2+/+}$ redox couple as opposed to the localized Ru(III/II) couple typical of classical ruthenium polypyridyl

Table 3. Electrochemical Data for Selected Complexes 1^{2+}–8^{+} Recorded in Acetonitrile (0.1 M Bu_4NPF_6) at a Glassy Carbon Working Electrode with Scan Rate 50 mV s^{-1}

	E° (V vs SCE)								
1^{2+}					1.29	−1.33	−1.52	−1.76	−2.38[a]
2^{+}				1.41[a]	0.52	−1.50	−1.74	−2.33[a]	−2.46[a]
3^{+}				1.27[a]	0.40	−1.52	−1.77	−2.31[a]	−2.50[a]
4^{+}				1.42[a]	0.44	−1.55	−1.87	−2.22	
5^{+}				1.35[a]	0.44	−1.57	−1.81	−2.35[a]	−2.54[a]
6^{+}				1.36[a]	0.44	−1.55	−1.79	−2.31[a]	−2.49[a]
7^{+}			1.65[a]	1.12	0.44	−1.51	−1.75	−2.29[a]	−2.45[a]
8^{+}	1.55[a]	1.08[a]		0.80	0.43	−1.33[a]	−1.51[a]	−1.82[a]	

[a]Irreversible.

dx.doi.org/10.1021/ic5002623 | Inorg. Chem. 2014, 53, 5556−5567

Scheme 2. Resonance Forms of the One-Electron Oxidized $[Ru(bpy)_2(OQN)]^{2+}$ and $[Ru(bpy)_2(R\text{-}OQN)]^{2+}$ Complexes Illustrating Their Noninnocent Character[a]

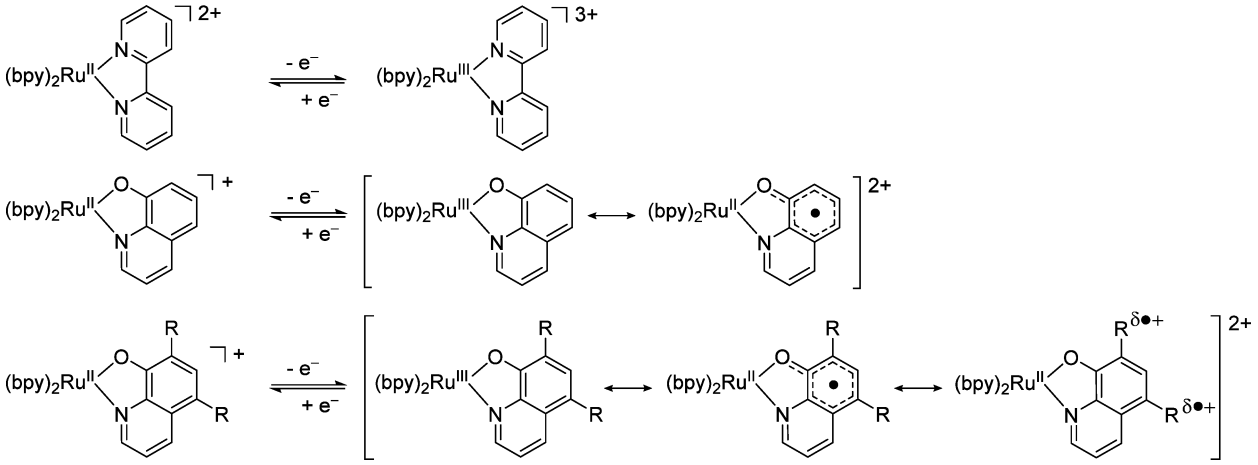

[a]R represents an additional electron-donating redox-active unit, e.g., methoxyphenyl or triphenylamine. It is noteworthy that the bpy unit in $[Ru(bpy)_3]^{3+}$ does not mix to any significant extent with the metal center resulting in a localized Ru^{III} oxidation state.

systems.[44] In fact DFT calculations show almost identical molecular orbital contributions for the HOMO and HOMO(β) of the monocationic and one-electron oxidized systems, respectively (Table 1, Supporting Information). Also common to the R-OQN series is an irreversible anodic peak occurring at potentials E° > +1.20 V versus SCE which, at least for complexes $\mathbf{2}^+$–$\mathbf{6}^+$, is most likely due to oxidation of the singly occupied Ru(dπ)–OQN(π) orbital of the dicationic derivatives. Complexes $\mathbf{7}^+$ and $\mathbf{8}^+$ display a more complex electrochemical response with additional redox couples observed as a result of the electron-donating *p*-methoxyphenyl and triphenylamine substituents. A single additional reversible redox couple is observed for complex $\mathbf{7}^+$ at E° = +1.12 V whereas complex $\mathbf{8}^+$ displays two additional quasireversible redox couples at +0.80 and +1.08 V suggesting both TPA subunits are capable of weakly coupled sequential one-electron oxidation events ($K_c \sim 5.4 \times 10^4$). Assignments of the one-electron oxidation products for dicationic complexes $\mathbf{2}^{2+}$–$\mathbf{8}^{2+}$ are discussed in further detail below using UV–vis–NIR and EPR monitored spectroelectrochemical data. Under a negative potential bias, complexes $\mathbf{2}^+$–$\mathbf{8}^+$ display a first reduction potential in the range E° = −1.49 to −1.56 V which is assigned as bpy(π*) reductions according to the DFT analysis discussed above. Apart from complex $\mathbf{8}^+$, this first reduction is comparable to the isoelectronic second bpy reduction of the monocationic reference derivative $\mathbf{1}^{+/0}$ (E° = −1.52 V). One-electron reduction of $\mathbf{8}^+$ at E° = −1.33 V shows non-Nernstian behavior indicative of adsorption of the neutral species **8** at the electrode surface precluding direct comparison with the remainder of the series. Substitution at the 2,4-positions in $\mathbf{4}^+$ appears to have an inductive donating influence as this system shows the most negative bpy(π*) reduction potential at E° = −1.49 V. In contrast, π-extension at the 5 or 5,7 positions of the OQN ligand appears to have little influence on the bpy(π*) LUMO level. Similarly, a second bpy(π*) reduction is observed in the potential range E° = −1.73 to −1.81 V which can be considered isoelectronic to the third bpy(π*) reduction of $\mathbf{1}^{0/-}$ observed at E° = −1.76 V. Due to the anionic nature of the R-OQN ligands they tend to display reduction potentials far negative of typical bpy(π*) reduction potentials. In fact, in a comparison of the fourth irreversible reduction peak observed for $\mathbf{1}^{-/2-}$ at E° = −2.38 V, it appears that the third reduction for complexes $\mathbf{2}^+$–$\mathbf{7}^+$ may also be bpy(π*) based occurring in the potential range E° = −2.29 to −2.35 V. A fourth irreversible anodic peak is observed for the R-OQN series in the range E° = −2.45 to −2.54 V possibly due to reduction of the electron rich R-OQN ligands.

EPR and UV–Vis–NIR Spectroelectrochemistry. To further probe the nature of the delocalized Ru(dπ)–OQN(π) HOMO energy level, controlled potential electrolysis was conducted while monitoring with UV–vis–NIR (room temperature) and electron paramagnetic resonance (EPR at 110 K) spectroscopies. These spectroelectrochemical methods are particularly informative for complexes $\mathbf{2}^{2+}$–$\mathbf{8}^{2+}$ as the in situ generated one-electron oxidized $[Ru(bpy)_2(R\text{-}OQN)]^{2+}$ complexes contain a singly occupied molecular orbital where the electron–hole may be delocalized across the Ru(dπ)–OQN(π) manifold and the peripheral electron donating substituents due to the noninnocent nature of this system (Scheme 2).

In fact, not only is spectroelectrochemistry of fundamental interest to inform on the electronic distribution in these complexes, but paramagnetic $4d^5$ ruthenium complexes are critical intermediates in a host of photochemical and redox based systems, most notably dye-sensitized solar cells.[62] Electron paramagnetic resonance is particularly powerful as a tool to map migration of the unpaired valence electron across the Ru(dπ)–OQN(π) framework, and beyond to the peripheral electron donating substituents. Here the *g*-anisotropy ($\Delta g = g_1 - g_3$) value provides a means to distinguish between metal and ligand centered radical species as it is strongly influenced by the amount of spin on a heavy atom (ruthenium in the present case) with its large spin–orbit coupling.[63,64] Therfore, by following the trend in *g*-anisotropy it is possible to identify the predominant resonance form contributing to the paramagnetic oxidation product in Scheme 2. Furthermore, this trend should also reflect the increasing contribution of ligand character to the HOMO orbital as earlier calculated by DFT (Table 1). All of the in situ electrochemically generated one-electron oxidized species ($\mathbf{1}^{3+}$–$\mathbf{8}^{2+}$) are EPR silent at 295 K due to significant contribution of ruthenium dπ orbitals to the singly occupied molecular orbital leading to fast relaxation times in fluid solutions. In a frozen

dx.doi.org/10.1021/ic5002623 | Inorg. Chem. 2014, 53, 5556–5567

glass at 110 K a rhombic *g*-anisotropy is observed for all complexes; however, 8^{2+} stands out in that it displays an unusually low value for its *g*-anisotropy ($\Delta g = 0.02$) due to the strong contribution of the electron rich triphenylamine groups to the singly occupied HOMO(β) level (Figure 9). Overall, the

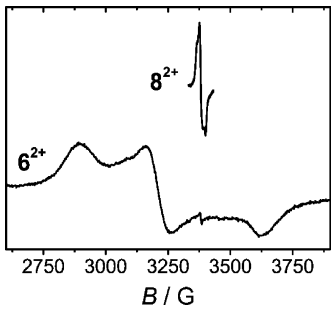

Figure 9. X-band EPR (9.48 GHz) spectroelectrochemical data for 6^{2+} and 8^{2+} (inset) recorded after in situ electrolysis in 0.1 M Bu_4NPF_6 acetonitrile electrolyte.

absolute value of Δg was found to be highly dependent on the nature of the R-OQN ligand, with values observed in the range 0.02−0.52 across the R-OQN series (Table 4). Even so these

Table 4. EPR Data of Complexes Following One-Electron Oxidation[a]

	g_1	g_2	g_3	Δg ($g_1 - g_3$)	g_{av}
1^{3+65}	2.64	2.64	1.14	1.50	2.14
2^{2+44}	2.37	2.10	1.86	0.51	2.12
3^{2+44}	2.30	2.10	1.89	0.41	2.10
4^{2+}	2.36	2.13	1.86	0.50	2.13
5^{2+}	2.37	2.10	1.85	0.52	2.11
6^{2+}	2.34	2.11	1.87	0.47	2.12
7^{2+}	2.28	2.09	1.89	0.39	2.09
8^{2+}	2.01	2.00	1.99	0.02	2.00

[a]Data were recorded at 110 K in acetonitrile 0.1 M Bu_4NPF_6 electrolyte following controlled potential electrolysis.

anisotropies are quite low and characteristic of significant R-OQN(π) contribution to the singly occupied HOMO(β) levels across the series from 2^{2+} to 8^{2+}, in contrast to the localized $4d^5$ ruthenium center in 1^{3+} which displays a *g*-anisotropy of Δg = 1.50. The trend observed for hole-delocalization across the Ru(dπ)−OQN(π) framework is further corroborated by theoretical Mulliken spin-density analysis as illustrated in Figure 10. While the *p*-methoxyphenyl substituent is not anticipated to be as electron-donating relative to the triphenylamine moiety it still displays the smallest *g*-anisotropy of Δg = 0.39 in the remainder of the series.

As the Ru(dπ)−OQN(π) HOMO level contributes significantly to visible electronic transitions for each of the monocationic complexes 2^+−8^+, upon one-electron oxidation characteristic electrochromism is observed upon formation of the dicationic derivatives 2^{2+}−8^{2+}. The most striking feature observed for the one-electron oxidized R-OQN complexes is generation of a broad NIR absorption band with λ_{max} ranging from 972 nm (ε = 1200 M^{-1} cm^{-1}, fwhm = 3573 cm^{-1}) for 2^{2+} to 1300 nm (ε = 16 000 M^{-1} cm^{-1}, fwhm = 2893 cm^{-1}) for 7^{2+}. This is in stark contrast to the weak ligand-to-metal charge transfer (LMCT) transition observed for $[Ru(bpy)_3]^{3+}$ (1^{3+}) in the visible region at 674 nm ($\varepsilon \sim 500$ M^{-1} cm^{-1}). UV−vis−

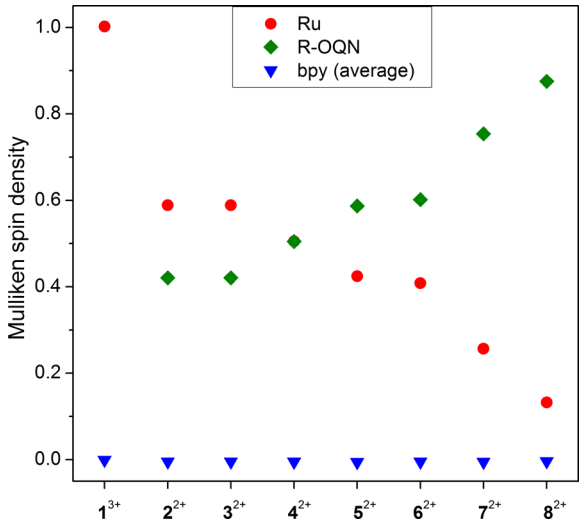

Figure 10. Mulliken spin-density analysis illustrating hole-delocalization onto the R-OQN ligands of 2^{2+}−8^{2+}, relative to the spin-localized $[Ru^{III}(bpy)_3]^{3+}$ system 1^{3+}. Spin-density on the bpy ligands is presented as an average value.

NIR electronic absorption spectra recorded during controlled potential electrolysis of the TPA_2OQN 8^+ complex is presented in Figure 11 with the complete set of UV−vis−NIR spectroelectrochemical data for complexes 1^{3+}−8^{2+} compiled in the Supporting Information, as well as spectra for the two-electron oxidized diamagnetic species 7^{3+} and 8^{3+}. In Figure 11 clean isosbestic points at 309, 388, 462, and 574 nm indicate a clean redox transformation from 8^+ to 8^{2+}. With depletion of the MLCT and MLLCT bands at 331 and 511 nm is a concerted grow in of relatively strong absorption bands at 415, 587, and 1300 nm. The NIR band at 1300 nm is especially broad with a fwhm of 2893 cm^{-1} due to three prominent underlying electronic transitions, confirmed by TD-DFT studies, each populating the LUMO(β) orbital and originating from the HOMO(β), HOMO − 1(β), and HOMO − 2(β) orbitals. Images of these contributing orbitals are included in Figure 11 where it can be clearly seen upon comparison with Figure 7 that the HOMO(β) orbital in 8^{2+} corresponds to the same delocalized Ru(dπ)−OQN(π) HOMO orbital found in the diamagnetic precursor 8^+. Thus, one-electron oxidation generates a paramagnetic species where the unpaired electron/electron−hole are delocalized across the Ru(dπ)−OQN(π) system as already implied by EPR analysis. Experimental data, TD-DFT spectra, electronic transition assignments, and electron density maps of contributing molecular orbitals are given in the Supporting Information for all one-electron oxidized complexes 1^{3+}−8^{2+} with a list of spectral data tabulated in Table 5. To summarize, the low energy NIR absorption bands observed for complexes 2^{2+}−6^{2+} are composed mainly of a π−π^* type transition involving the delocalized Ru(dπ)−OQN(π) system. Upon introduction of the *p*-methoxyphenyl and triphenylamine substituents in 7^{2+} and 8^{2+} an enhanced OQN(π) → [Ru(dπ)−OQN(π)] charge-transfer character is introduced corresponding to a bathochromic shift and amplified extinction coefficient with increasing π-extension and electron rich character (Figure 12).

CONCLUSIONS

The influence of π-extension and electron rich $n \rightarrow \pi$ donation has been explored at the noninnocent Ru(dπ)−OQN(π)

dx.doi.org/10.1021/ic5002623 | Inorg. Chem. 2014, 53, 5556−5567

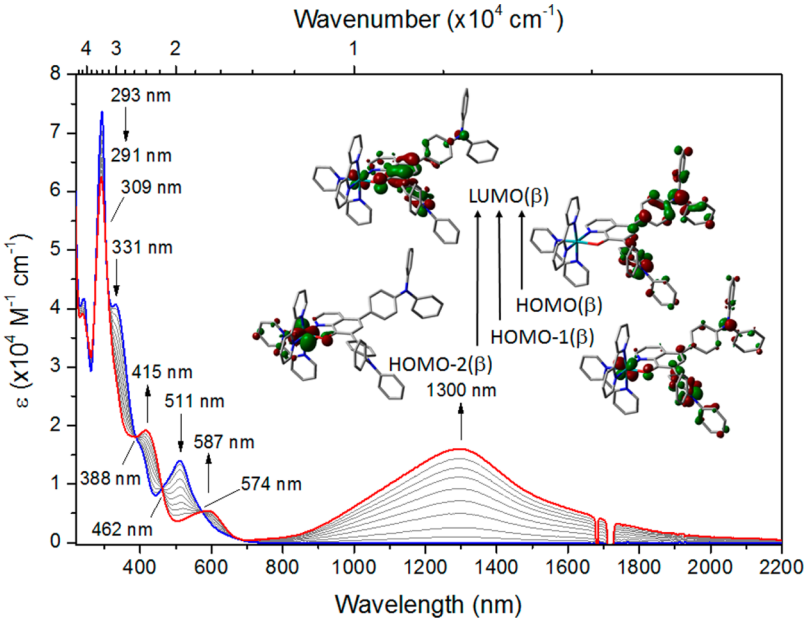

Figure 11. UV−vis−NIR electronic absorption data of 8^{2+} recorded during controlled potential electrolysis (+0.65 V vs SCE) of 8^{+} in 0.1 M Bu_4NPF_6 acetonitrile electrolyte. Molecular orbitals contributing to the NIR absorption band of 8^{2+} are also shown.

Table 5. UV−Vis−NIR Electronic Absorption Data for Complexes 1^{3+}−8^{2+}

	absorption[a] λ_{max} (nm); ($\varepsilon \times 10^4$ M^{-1} cm^{-1})
1^{3+}	250 (4.15), 304 (4.27), 314 (4.20), 421 (0.25), 674 (0.05)
2^{2+}	249 (4.63), 292 (3.80), 367 (0.86), 502 (0.71), 972 (0.12)
3^{2+}	254 (3.57), 286 (3.60), 373 (0.68), 510 (0.49), 1055 (0.33)
4^{2+}	248 (2.70), 287 (3.50), 415 (0.67), 1030 (0.27)
5^{2+}	253 (4.42), 286 (3.89), 371 (0.89), 505 (0.61), 1064 (0.38)
6^{2+}	248 (3.80), 282 (5.60), 384 (0.92), 513 (0.47), 556 (0.39), 1092 (0.61)
7^{2+}	251 (447), 284 (5.96), 390 (1.09), 544 (0.47), 571 (0.47), 739 (0.21), 1147 (1.18)
8^{2+}	239 (3.91), 293 (6.25), 415 (1.92), 587 (0.55), 1300 (1.60)

[a]Recorded at room temperature in 0.1 M Bu_4NPF_6 acetonitrile electrolyte following controlled potential electrolysis.

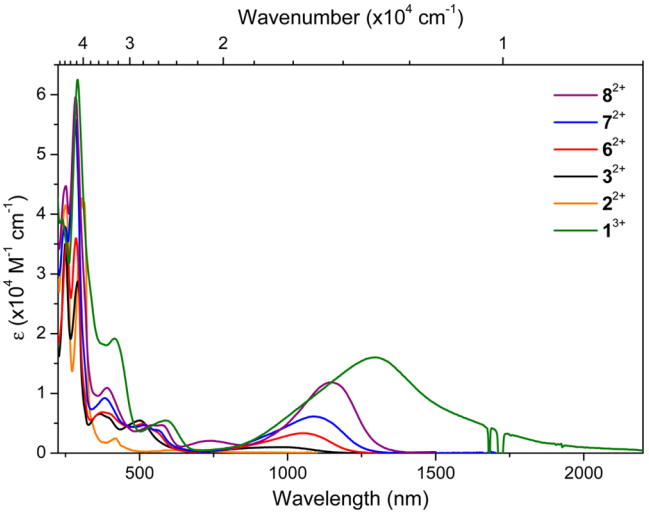

Figure 12. Overlay of UV−vis−NIR electronic absorption data recorded following controlled potential electrolysis of 1^{3+} and complexes 2^{2+}, 3^{2+}, 6^{2+}, 7^{2+}, and 8^{2+} in 0.1 M Bu_4NPF_6 acetonitrile electrolyte.

system where, by enhancing the electron-donating character of the R-OQN ligand, increased mixing of Ru(dπ) atomic and OQN(π) molecular orbitals is observed. Electronic structures have been probed experimentally by a combination of electrochemical and spectroscopic techniques (UV−vis−NIR absorption, emission, EPR) where a combination of metal-to-ligand (MLCT) and (metal−ligand)-to-ligand (MLLCT) charge-transfer electronic transitions are found to be consistent with time dependent-density functional theory (TD-DFT) analysis, and responsible for the panchromatic visible absorption spectra and enhanced light harvesting properties for these systems. An added consequence of the Ru(dπ)−OQN(π) bonding interaction is the multiple redox states made accessible through functionalization of the OQN ligand with the 5,7-bis(4-methoxyphenyl) and 5,7-bis(4-(diphenylamino)-phenyl) redox active moieties. Extensive charge delocalization is observed for the one-electron oxidized systems 2^{2+}−8^{2+} using a combination of UV−vis−NIR, EPR spectroelectrochemistry and Mulliken spin-density analysis, giving strong evidence for hole-delocalization across the entire Ru(dπ)−OQN(π) system, in particular for the electron-rich 5,7-bis(4-methoxyphenyl) and 5,7-bis(4-(diphenylamino)phenyl) systems 7^{2+} and 8^{2+}. Work is currently underway to investigate the potential of this class of chromophore in a photovoltaic device for n-type semiconductor sensitization. Furthermore, the noninnocent bonding model put forth for $[Ru(bpy)_2(R\text{-}OQN)]^{+}$ systems will in future be applied to a wider range of isoelectronic noninnocent ligand systems to better understand their redox, photophysical, and photoelectrochemical properties.

EXPERIMENTAL SECTION

Physical Measurements. ^1H NMR spectra were recorded on a Varian spectrometer operating at 300.13 MHz for ^1H and 75.03 MHz for ^{13}C nuclei. Deuterated solvents were purchased from Aldrich, and residual proton signals were used as an internal reference point for reporting the chemical shift (δ) in *d*-chloroform (δ (^1H) = 7.26 ppm, δ (^{13}C) = 77.16 ppm), d_6-acetone (δ (^1H) = 2.05 ppm, δ (^{13}C) = 29.84, 206.26 ppm), and d_6-dimethyl sulfoxide (δ (^1H) = 2.50 ppm, δ (^{13}C) = 39.52 ppm).[66] Mass spectroscopy was carried out on a Thermo

dx.doi.org/10.1021/ic5002623 | Inorg. Chem. 2014, 53, 5556−5567

Finnigan electrospray ionization mass spectrometer (ESI-MS). Elemental analysis was conducted with a PerkinElmer 2400 instrument. Cyclic voltammetry was carried out on a CH Instruments 620D potentiostat. A standard three electrode cell was used under an atmosphere of argon with 0.1 M Bu_4NPF_6 in spectrophotometric grade acetonitrile as the supporting electrolyte. Glassy carbon (3 mm diameter) and Pt wire were used as working and counter electrodes, respectively. A nonaqueous reference electrode was used to minimize IR drop at the solvent interface. This consisted of a Ag wire in the same supporting electrolyte separated by a vycor frit. All experiments were calibrated using ferrocene as an internal pseudoreference due to the relative instability of the reference electrode employed. All redox potentials are reported in reference to the saturated calomel electrode (SCE) which has been reported at 0.40 V negative of the $Fc^{+/0}$ couple under identical conditions.[67] The formal redox potential E° was determined from cyclic voltammetry as $(E_{pa} + E_{pc})/2$, where E_{pa} and E_{pc} are the anodic and cathodic peak potentials, respectively. Where E° could not be calculated due to irreversible behavior, potentials are reported as either the E_{pa} minimar or E_{pc} maxima. UV−vis absorption spectra were recorded on an Agilent 8456 diode array spectrophotometer in spectrophotometric grade acetonitrile. UV−vis−NIR spectroelectrochemical experiments were conducted using a Varian Cary 500 Scan spectrophotometer in tandem with a custom spectroelectrochemical flow cell whose design is based upon a literature description.[68] This consisted of a Pt-foil/gauze working electrode and Pt-gauze counter electrode (isolated via a fine porosity glass frit). The same Ag-wire reference electrode was again used for controlled potential electrolysis experiments. Electron paramagnetic resonance (EPR) measurements were made in a two-electrode capillary tube with an X-band (9.48 GHz) Bruker System EMX at a low temperature of 110 K. All of the in situ electrochemically generated one-electron oxidized species ($\mathbf{1}^{2+}$−$\mathbf{8}^{2+}$) in CH_3CN/0.1 M Bu_4NPF_6 are EPR silent at 295 K due to significant contribution of ruthenium dπ orbitals to the singly occupied molecular orbital leading to fast relaxation times, and EPR silence in fluid solutions.

Computational Details. All calculations were carried out using density functional theory (DFT) with the B3LYP functional as implemented in the Gaussian 09 program package.[69] The LANL08 basis set[70] was used for Ru, and 6-31G(d,p) is used for other elements.[71,72] The optimization calculations were carried out using the polarizable continuum model (PCM) with the dielectric constant of acetonitrile.[73] A vibrational frequency analysis coupling with PCM model was carried out in order to confirm the minimum-energy geometry in solution, followed by time-dependent density functional theory (TD-DFT).[74] Doublet species were calculated using an unrestricted spin approach.

Materials. Tetrakis(triphenylphosphine)palladium, 10% palladium on charcoal, 4-methoxyphenylboronic acid, 4-(diphenylamino)-phenylboronic acid, 1,4-cyclohexadiene, potassium carbonate, potassium hydroxide, potassium hexafluorophosphate, Celite, and acetonitrile (spectrophotometric grade, Aldrich) were purchased from Aldrich and used as received. ACS reagent grade solvents methanol, acetone, acetonitrile, and diethyl ether (Pharmco) were used as received. Tetrabutylammonium hexafluorophsophate (Aldrich) was recrystallized thrice from hot ethanol prior to use. Compounds 5,7-diiodo-8-benzyloxyquinoline,[75] 5-phenyl-8-hydroxyquinoline,[52] 5,7-diphenyl-8-hydroxyquinoline,[52] $Ru(bpy)_2Cl_2$,[76] $\mathbf{2}^+$, and $\mathbf{3}^{+44}$ were prepared according to literature methods.

General Method for Synthesis of Benzyl Protected R-OQN Ligands. To an argon degassed 20 mL solution of toluene/ethanol/water (2:1:1) was added 0.73 g (1.5 mmol) of 5,7-diiodo-8-benzyloxyquinoline, 3.5 mmol of the appropriate boronic acid, 0.97 g (7 mmol) of potassium carbonate, and 0.74 g (0.6 mmol) of tetrakis(triphenylphosphine)palladium. The reaction mixture was refluxed under an argon atmosphere with stirring for 12 h. Upon cooling 30 mL of dichloromethane was added, and the organic phase was washed with water and brine and dried over $MgSO_4$. Dichloromethane was subsequently removed ex vacuo, and the benzyloxy protected ligand precursor was precipitated from hot methanol. The 5,7-substituted 8-hydroxyquinoline ligand was isolated according to a reported procedure by refluxing the benzyloxy protected precursor (2 mmol) in ethanol overnight under an argon atmosphere with 1,4-cyclohexadiene (20 mmol) and 0.5 g of 10% palladium on carbon. After cooling the crude mixture was passed through a Celite plug with excess dichloromethane. Analytically pure ligand was recovered following removal of the dichloromethane ex vacuo and recrystallization from hot methanol.

5,7-Bis(4-methoxyphenyl)-8-benzyloxyquinoline. This was synthesized in 84% yield. ^{1}H NMR δ[$CDCl_3$]: 3.83−3.85 (m, 6H), 5.12 (s, 2H), 6.96 (d, 2H, J = 1.2 Hz), 7.02 (d, 2H, J = 1.2 Hz), 7.22−7.24 (m, 5H), 7.35 (dd, 1H, J = 4.0, 9.0 Hz), 7.39 (d, 2H, J = 9.0 Hz), 7.62 (s, 1H), 7.64 (d, 2H, J = 9.0 Hz), 8.25 (m, 1H), 8.97 (m, 1H) ppm. ^{13}C NMR δ[$CDCl_3$]: 55.42, 76.19, 113.69, 113.99, 114.69, 116.30, 120.89, 127.27, 127.66, 128.03, 128.60, 129.70, 130.55, 131.15, 131.22, 131.62, 133.60, 134.69, 135.69, 137.52, 143.66, 149.70, 150.69, 159.09, 159.21 ppm. ESI-MS [M + H^+] m/z: calcd 448.1913; obsd 448.1277.

5,7-Bis(4-diphenylamino)phenyl-8-benzyloxyquinoline. This was synthesized in 72% yield. ^{1}H NMR δ[$CDCl_3$]: 5.22 (s, 2H), 7.03−7.09 (m, 5H), 7.13−7.20 (m, 12H), 7.25−7.31 (m, 9H), 7.36 (d, 4H, J = 4.8 Hz), 7.40 (dd, 1H, J = 2.7, 5.1 Hz), 7.60 (d, 4H, J = 4.5 Hz), 8.36 (d, 1H, J = 5.4 Hz), 9.10 (d, 1H, J = 3.0 Hz) ppm. ^{13}C NMR δ[$CDCl_3$]: 11.12, 14.20, 23.10, 23.89, 24.60, 29.04, 29.83, 30.52, 34.13, 38.83, 66.91, 76.49, 120.95, 123.00, 123.25, 123.37, 123.44, 124.47, 124.71, 127.24, 127.26, 128.14, 128.71, 129.38, 129.47, 129.59, 130.96, 132.25, 133.09, 133.79, 134.76, 135.75, 137.76, 143.76, 147.17, 147.46, 147.73, 147.81, 149.80, 150.88, 199.59, 215.98 ppm. ESI-MS [M + H^+] m/z: calcd 722.3171; obsd 722.2783.

Deprotection of R-OQN Ligands. The 5,7-substituted 8-hydroxyquinoline ligand was isolated according to a reported procedure by refluxing the benzyloxy protected precursor (2 mmol) in ethanol overnight under an argon atmosphere with 1 g (12 mmol) of 1,4-cyclohexadiene and 0.5 g of 10% palladium on carbon. After cooling, the crude mixture was passed through a Celite plug with excess dichloromethane. Analytically pure ligand was recovered following removal of the dichloromethane ex vacuo and recrystallization from hot methanol.

5,7-Bis(4-methoxyphenyl)-8-hydroxyquinoline. This was synthesized in 91% yield. ^{1}H NMR δ[d_6-DMSO]: 3.82 (s, 3H), 3.84 (s, 3H), 6.67 (d, 2H, J = 5.4 Hz), 6.74 (d, 2H, J = 5.4 Hz), 7.46 (d, 2H, J = 5.4 Hz), 7.49 (s, 1H), 7.57 (dd, 1H, J = 2.7, 5.1 Hz), 7.75 (d, 2H, J = 5.4 Hz), 7.62 (s, 1H), 8.25 (dd, 1H, J = 0.9, 5.1 Hz), 8.92 (dd, 1H, J = 0.9, 2.4 Hz), 9.85 (s, 1H) ppm. ESI-MS [M + H^+] m/z: calcd 358.1443; obsd 358.1311.

5,7-Bis(4-diphenylamino)phenyl-8-hydroxyquinoline. This was synthesized in 82% yield. ^{1}H NMR δ[$CDCl_3$]: 7.00−7.42 (m, 25H), 7.63 (s, 2H), 7.55 (d, 4H, J = 9.0 Hz), 8.42 (d, 1H, J = 8.1 Hz), 8.81 (s, 1H) ppm. ^{13}C NMR δ[$CDCl_3$]: 11.12, 14.21, 23.11, 23.89, 24.60, 28.51, 29.04, 29.84, 30.52, 34.14, 38.83, 66.95, 115.43, 116.38, 117.69, 121.49, 121.88, 121.96, 122.77, 122.92, 123.02, 123.15, 123.56, 123.60, 124.26, 124.62, 125.75, 127.65, 129.17, 129.38, 129.46, 129.73, 130.20, 130.46, 130.91, 131.57, 133.29, 134.82, 138.85, 147.02, 147.21, 147.79, 147.93, 199.58, 216.00 ppm. ESI-MS [M + H^+] m/z: calcd 632.2702; obsd 632.2617.

General Synthetic Method for $[Ru(bpy)_2(R\text{-}OQN)][PF_6]$ Complexes ($\mathbf{4}^+$−$\mathbf{8}^+$). A 50 mL flask was charged with 10 mL of methanol and the solution purged with argon for 10 min. To the flask was added 0.10 mmol of $Ru(bpy)_2Cl_2\cdot 2H_2O$, 0.11 mmol of the appropriately substituted hydroxyquinoline, and 1.1 mL of 0.1 M aqueous potassium hydroxide. With an argon atmosphere maintained, the purple suspension was allowed to reflux with stirring for 5 h resulting in a deep reddish/brown solution. The methanol was then removed on a rotary evaporator resulting in a crude aqueous solution of the $[Ru(bpy)_2(R\text{-}OQN)]Cl$ salt. Additional water was added (5 mL), the pH was adjusted to 7 using 0.1 M aqueous HCl, and the trace unreacted ligand was removed by gravity filtration. To the deep red homogeneous filtrate was added dropwise 1 M aqueous KPF_6 until a dark reddish brown precipitate developed. The solid was isolated by vacuum filtration on a medium porosity sintered funnel. Recrystalliza-

dx.doi.org/10.1021/ic5002623 | Inorg. Chem. 2014, 53, 5556−5567

tion from acetone and diethyl ether consistently resulted in analytically pure product in 70−80% yield.

4^{+}, *[Ru(bpy)$_2$(PhOQN)](PF$_6$)*. ^{1}H NMR δ[(CD$_3$)$_2$CO]: 6.89 (d, 1H, J = 8.4 Hz), 7.23 (dd, 1H, J = 3.9, 4.8 Hz), 7.34−7.52 (m, 9H), 7.62 (dd, 1H, J = 1.2, 2.4 Hz), 7.68−7.73 (m, 1H), 7.91 (d, 1H, J = 5.4 Hz), 8.00−8.20 (m, 7H), 8.70−8.77 (m, 4H), 8.95 (d, 1H, J = 5.7 Hz) ppm. ESI-MS [M − PF$_6^-$] m/z: calcd 634.1; obsd 634.2. Anal. Calcd for $C_{35}H_{26}F_6N_5OPRu$: C 53.99%; H 3.37%; N 8.99%. Found: C 53.31%; H 3.82%; N 8.76%.

5^{+}, *[Ru(bpy)$_2$(i-Ph$_2$OQN)](PF$_6$)*. ^{1}H NMR δ[(CD$_3$)$_2$CO]: 6.78−6.82 (m, 1H), 6.86−6.89 (m, 1H), 6.93−6.99 (m, 2H), 7.04 (s, 1H), 7.24−7.36 (m, 3H), 7.44−7.46 (m, 1H), 7.52−7.64 (m, 11H), 7.71−7.76 (m, 1H), 7.87−7.93 (m, 1H), 8.04−8.10 (m, 1H), 8.21−8.28 (m, 2H), 8.46−8.48 (m, 1H), 8.52−8.55 (m, 1H), 8.64−8.71 (m, 2H), 8.83−8.86 (m, 1H) ppm. ESI-MS [M − PF$_6^-$] m/z: calcd 710.1; obsd 710.1. Anal Calcd for $C_{41}H_{30}F_6N_5OPRu$: C 57.61%; H 3.54%; N 8.19%. Found: C 57.01%; H 4.02%; N 7.54%.

6^{+}, *[Ru(bpy)$_2$(Ph$_2$OQN)](PF$_6$)*. ^{1}H NMR δ[(CD$_3$)$_2$CO]: 7.13 (d, 1H, J = 7.2 Hz), 7.20−7.26 (m, 2H), 7.36−7.53 (m, 6H), 7.63 (s, 1H), 7.65−7.73 (m, 2H), 7.85−7.92 (m, 2H), 7.97−8.20 (m, 8H), 8.64−8.78 (m, 4H), 8.97 (d, 1H, J = 5.1 Hz) ppm. ESI-MS [M − PF$_6^-$] m/z: calcd 710.1; obsd 710.2. Anal. Calcd for $C_{41}H_{30}F_6N_5OPRu$: C 57.61%; H 3.54%; N 8.19%. Found: C 56.33%; H 3.91%; N 7.89%.

7^{+}, *{Ru(bpy)$_2$[(MeOPh)$_2$OQN]}(PF$_6$)*. ^{1}H NMR δ[(CD$_3$)$_2$CO]: 2.85 (s, 3H), 2.88 (s, 3H), 6.89 (d, 1H, J = 9.0 Hz), 7.00−7.15 (m, 6H), 7.21−7.50 (m, 8H), 7.65 (d, 1H, J = 3.0 Hz), 7.69−7.73 (m, 2H), 7.92 (d, 2H, J = 9.0 Hz), 7.96−8.09 (m, 4H), 8.24 (d, 1H, J = 6.0 Hz), 8.65 (d, 1H, J = 6.0 Hz), 8.70−8.79 (m, 3H), 8.96 (d, 1H, J = 6.0 Hz) ppm. ESI-MS [M − PF$_6^-$] m/z: calcd 770.2; obsd 770.2. Anal. Calcd for $C_{43}H_{34}F_6N_5O_3PRu$: C 56.46%; H 3.75%; N 7.66%. Found: C 56.02%; H 3.98%; N 7.12%.

8^{+}, *[Ru(bpy)$_2$(TPA$_2$OQN)](PF$_6$)*. ^{1}H NMR δ[(CD$_3$)$_2$CO]: 6.83−6.86 (m, 2H), 6.92−7.24 (m, 19H), 7.30−7.43 (m, 8H), 7.62−7.71 (m, 3H), 7.84−7.95 (m, 6H), 7.95−8.03 (m, 1H), 8.08−8.14 (m, 3H), 8.24 (dd, 1H, J = 1.2, 12.0 Hz), 8.52−8.59 (m, 2H), 8.70−8.77 (m, 2H), 9.01 (d, 1H, J = 5.1 Hz) ppm. ESI-MS [M − PF$_6^-$] m/z: calcd 1044.3; obsd 1044.4. Anal. Calcd for $C_{65}H_{48}F_6N_7OPRu$: C 65.65%; H 4.07%; N 8.25%. Found: C 65.12%; H 4.52%; N 7.99%.

■ ASSOCIATED CONTENT

Supporting Information

UV−vis electronic absorption spectra, excitation and emission spectra, cyclic voltammetry, UV−vis−NIR spectroelectrochemistry, computational data, Cartesian coordinates, and complete ref 69. This material is available free of charge via the Internet at http://pubs.acs.org.

■ AUTHOR INFORMATION

Corresponding Authors

*E-mail: mktsai@ntnu.edu.tw.

*E-mail: jonathan.rochford@umb.edu.

Author Contributions

The manuscript was written through contributions of all authors. All authors have given approval to the final version of the manuscript.

Notes

The authors declare no competing financial interest.

■ ACKNOWLEDGMENTS

J.R. thanks University of Massachusetts—Boston for financial support. The authors thank the Fonds der Chemischen Industrie (FCI) for providing a doctoral stipend (Chemiefondsstipendium) to D.S. T.-C.C. and M.-K.T. are supported by the National Science Council of Taiwan (Grants 99-2113-M-003-007-MY2 and 101-2113-M-003-003-MY2), and are grateful to the National Center for High-Performance Computing for computer time and facilities.

■ REFERENCES

(1) Romain, S.; Vigara, L.; Llobet, A. *Acc. Chem. Res.* **2009**, *42*, 1944−1953.
(2) Concepcion, J. J.; Jurss, J. W.; Brennaman, M. K.; Hoertz, P. G.; Patrocinio, A. O. T.; Murakami Iha, N. Y.; Templeton, J. L.; Meyer, T. J. *Acc. Chem. Res.* **2009**, *42*, 1954−1965.
(3) Chen, Z.; Chen, C.; Weinberg, D. R.; Kang, P.; Concepcion, J. J.; Harrison, D. P.; Brookhart, M. S.; Meyer, T. J. *Chem. Commun.* **2011**, *47*, 12607−12609.
(4) Windle, C. D.; Perutz, R. N. *Coord. Chem. Rev.* **2012**, *256*, 2562−2570.
(5) Wang, C.; Ma, X.-X.; Li, J.; Xu, L.; Zhang, F.-x. *J. Mol. Catal. A: Chem.* **2012**, *363*, 108−114.
(6) Suzuki, T. M.; Nakamura, T.; Saeki, S.; Matsuoka, Y.; Tanaka, H.; Yano, K.; Kajino, T.; Morikawa, T. *J. Mater. Chem.* **2012**, *22*, 24584−24590.
(7) Ohtsu, H.; Tanaka, K. *Angew. Chem., Int. Ed.* **2012**, *51*, 9792−9795.
(8) Anderson, S.; Constable, E. C.; Dare-Edwards, M. P.; Goodenough, J. B.; Hamnett, A.; Seddon, K. R.; Wright, R. D. *Nature* **1979**, *280*, 571−573.
(9) Ardo, S.; Meyer, G. J. *Chem. Soc. Rev.* **2009**, *38*, 115−164.
(10) Johansson, P. G.; Zhang, Y.; Abrahamsson, M.; Meyer, G. J.; Galoppini, E. *Chem. Commun.* **2011**, *47*, 6410−6412.
(11) Heuer, W. B.; Xia, H.-L.; Ward, W.; Zhou, Z.; Pearson, W. H.; Siegler, M. A.; Narducci Sarjeant, A. A.; Abrahamsson, M.; Meyer, G. J. *Inorg. Chem.* **2012**, *51*, 3981−3988.
(12) Coe, B. J.; Harris, J. A.; Brunschwig, B. S.; Asselberghs, I.; Clays, K.; Garin, J.; Orduna, J. *J. Am. Chem. Soc.* **2005**, *127*, 13399−13410.
(13) Coe, B. J. *Acc. Chem. Res.* **2006**, *39*, 383−393.
(14) Gauthier, N.; Argouarch, G.; Paul, F.; Toupet, L.; Ladjarafi, A.; Costuas, K.; Halet, J.-F.; Samoc, M.; Cifuentes, M. P.; Corkery, T. C.; Humphrey, M. G. *Chem.—Eur. J.* **2011**, *17*, 5561−5577.
(15) Kalyanasundaram, K. *Coord. Chem. Rev.* **1982**, *46*, 159−244.
(16) McCusker, C. E.; McCusker, J. K. *Inorg. Chem.* **2011**, *50*, 1656−1669.
(17) Campagna, S.; Puntoriero, F.; Nastasi, F.; Bergamini, G.; Balzani, V. *Photochemistry and Photophysics of Coordination Compounds: Ruthenium*; Springer-Verlag: Berlin, 2007; Vol. *280*, pp 117−214.
(18) Juris, A.; Balzani, V.; Barigelletti, F.; Campagna, S.; Belser, P.; Vonzelewsky, A. *Coord. Chem. Rev.* **1988**, *84*, 85−277.
(19) England, J.; Scarborough, C. C.; Weyhermueller, T.; Sproules, S.; Wieghardt, K. *Eur. J. Inorg. Chem.* **2012**, 4605−4621.
(20) Kober, E. M.; Meyer, T. J. *Inorg. Chem.* **1982**, *21*, 3967−3977.
(21) Daul, C.; Baerends, E. J.; Vernooijs, P. *Inorg. Chem.* **1994**, *33*, 3538−3543.
(22) Ward, M. D.; McCleverty, J. A. *J. Chem. Soc., Dalton. Trans.* **2002**, 275−288.
(23) Kaim, W.; Sarkar, B. *Coord. Chem. Rev.* **2007**, *251*, 584−594.
(24) Ray, K.; Petrenko, T.; Wieghardt, K.; Neese, F. *Dalton Trans.* **2007**, 1552−1566.
(25) Kaim, W.; Schwederski, B. *Coord. Chem. Rev.* **2010**, *254*, 1580−1588.
(26) Eisenberg, R. *Coord. Chem. Rev.* **2011**, *255*, 825−836.
(27) Kaim, W. *Inorg. Chem.* **2011**, *50*, 9752−9765.
(28) de Bruin, B. *Eur. J. Inorg. Chem.* **2012**, 340−342.
(29) Lyaskovskyy, V.; de Bruin, B. *ACS Catal.* **2012**, *2*, 270−279.
(30) Kaim, W. *Eur. J. Inorg. Chem.* **2012**, 343−348.
(31) Chan, S.-C.; England, J.; Lee, W.-C.; Wieghardt, K.; Wong, C.-Y. *ChemPlusChem* **2013**, *78*, 214−217.
(32) Kar, S.; Sarkar, B.; Ghumaan, S.; Leboschka, M.; Fiedler, J.; Kaim, W.; Lahiri, G. K. *Dalton Trans.* **2007**, 1934−1938.
(33) Das, A.; Scherer, T. M.; Mondal, P.; Mobin, S. M.; Kaim, W.; Lahiri, G. K. *Chem.—Eur. J.* **2012**, *18*, 14434−14443.
(34) Boyer, J. L.; Rochford, J.; Tsai, M. K.; Muckerman, J. T.; Fujita, E. *Coord. Chem. Rev.* **2010**, *254*, 309−330.

(35) Zhao, H. C.; Harney, J. P.; Huang, Y.-T.; Yum, J.-H.; Nazeeruddin, M. K.; Grätzel, M.; Tsai, M.-K.; Rochford, J. *Inorg. Chem.* **2011**, *51*, 1−3.
(36) Robson, K. C. D.; Bomben, P. G.; Berlinguette, C. P. *Dalton Trans.* **2012**, *41*, 7814−7829.
(37) Bhattacharya, S. *Polyhedron* **1993**, *12*, 235−239.
(38) Warren, J. T.; Chen, W.; Johnston, D. H.; Turro, C. *Inorg. Chem.* **1999**, *38*, 6187−6192.
(39) Warren, J. T.; Johnston, D. H.; Turro, C. *Inorg. Chem. Commun.* **1999**, *2*, 354−357.
(40) Leung, C.-F.; Wong, C.-Y.; Ko, C.-C.; Yuen, M.-C.; Wong, W.-T.; Wong, W.-Y.; Lau, T.-C. *Inorg. Chim. Acta* **2009**, *362*, 1149−1157.
(41) Sears, R. B.; Joyce, L. E.; Turro, C. *J. Photochem. Photobiol.* **2010**, *86*, 1230−1236.
(42) El Ojaimi, M.; Thummel, R. P. *Inorg. Chem.* **2011**, *50*, 10966−10973.
(43) Tong, L.; Wang, Y.; Duan, L.; Xu, Y.; Cheng, X.; Fischer, A.; Ahlquist, M. S. G.; Sun, L. *Inorg. Chem.* **2012**, *51*, 3388−3398.
(44) Zhao, H. C.; Fu, B.-L.; Schweinfurth, D.; Harney, J. P.; Sarkar, B.; Tsai, M.-K.; Rochford, J. *Eur. J. Inorg. Chem.* **2013**, *2013*, 4410−4420.
(45) Qin, Y.; Kiburu, I.; Shah, S.; Jakle, F. *Org. Lett.* **2006**, *8*, 5227−5230.
(46) Qin, Y.; Kiburu, I.; Shah, S.; Jäkle, F. *Macromolecules* **2006**, *39*, 9041−9048.
(47) Heiskanen, J. P.; Hormi, O. E. O. *Tetrahedron* **2009**, *65*, 518−524.
(48) Heiskanen, J. P.; Hormi, O. E. O. *Tetrahedron* **2009**, *65*, 8244−8249.
(49) Perez-Bolivar, C.; Llovera, L.; Lopez, S. E.; Anzenbacher, P., Jr. *J. Lumin.* **2010**, *130*, 145−152.
(50) Perez-Bolivar, C.; Takizawa, S. Y.; Nishimura, G.; Montes, V. A.; Anzenbacher, P. *Chem.—Eur. J.* **2011**, *17*, 9076−9082.
(51) Zlojutro, V.; Sun, Y.; Hudson, Z. M.; Wang, S. *Chem. Commun.* **2011**, *47*, 3837−3839.
(52) Shoji, E.; Miyatake, K.; Hlil, A. R.; Hay, A. S.; Maindron, T.; Jousseaume, V.; Dodelet, J. P.; Tao, Y.; D'Iorio, M. *J. Polym. Sci., Part A: Polym. Chem.* **2003**, *41*, 3006−3016.
(53) Kulkarni, A.; Torok, B. *Green Chem.* **2010**, *12*, 875−878.
(54) McClure, B. A.; Rack, J. J. *Eur. J. Inorg. Chem.* **2010**, 3895−3904.
(55) Suzuki, K.; Kobayashi, A.; Kaneko, S.; Takehira, K.; Yoshihara, T.; Ishida, H.; Shiina, Y.; Oishic, S.; Tobita, S. *Phys. Chem. Chem. Phys.* **2009**, *11*, 9850−9860.
(56) Caspar, J. V.; Meyer, T. J. *J. Am. Chem. Soc.* **1983**, *105*, 5583−5590.
(57) O'Donnell, R. M.; Johansson, P. G.; Abrahamsson, M.; Meyer, G. J. *Inorg. Chem.* **2013**, *52*, 6839−6848.
(58) Sun, Q.; Mosquera-Vazquez, S.; Lawson Daku, L. M.; Guénée, L.; Goodwin, H. A.; Vauthey, E.; Hauser, A. *J. Am. Chem. Soc.* **2013**, *135*, 13660−13663.
(59) Durham, B.; Caspar, J. V.; Nagle, J. K.; Meyer, T. J. *J. Am. Chem. Soc.* **1982**, *104*, 4803−4810.
(60) Cherry, W. R.; Henderson, L. J. *Inorg. Chem.* **1984**, *23*, 983−986.
(61) Treadway, J. A.; Loeb, B.; Lopez, R.; Anderson, P. A.; Keene, F. R.; Meyer, T. J. *Inorg. Chem.* **1996**, *35*, 2242−2246.
(62) Hu, K.; Robson, K. C. D.; Johansson, P. G.; Berlinguette, C. P.; Meyer, G. J. *J. Am. Chem. Soc.* **2012**, *134*, 8352−8355.
(63) Patra, S.; Sarkar, B.; Mobin, S. M.; Kaim, W.; Lahiri, G. K. *Inorg. Chem.* **2003**, *42*, 6469−6473.
(64) Weisser, F.; Huebner, R.; Schweinfurth, D.; Sarkar, B. *Chem.—Eur. J.* **2011**, *17*, 5727−5736.
(65) DeSimone, R. E.; Drago, R. S. *J. Am. Chem. Soc.* **1970**, *92*, 2343−2352.
(66) Fulmer, G. R.; Miller, A. J. M.; Sherden, N. H.; Gottlieb, H. E.; Nudelman, A.; Stoltz, B. M.; Bercaw, J. E.; Goldberg, K. I. *Organometallics* **2010**, *29*, 2176−2179.
(67) Connelly, N. G.; Geiger, W. E. *Chem. Rev.* **1996**, *96*, 877−910.
(68) Fajer, J.; Fujita, I.; Davis, M. S.; Forman, A.; Hanson, L. K.; Smith, K. M. *Adv. Chem. Ser.* **1982**, 489−513.
(69) Frisch, M. J.; et al. *Gaussian 09, Revision A.1*; Gaussian Inc.: Wallingford, CT, 2009.
(70) Roy, L. E.; Hay, P. J.; Martin, R. L. *J. Chem. Theory Comput.* **2008**, *4*, 1029−1031.
(71) Harihara, Pc; Pople, J. A. *Theor. Chim. Acta* **1973**, *28*, 213−222.
(72) Francl, M. M.; Pietro, W. J.; Hehre, W. J.; Binkley, J. S.; Gordon, M. S.; Defrees, D. J.; Pople, J. A. *J. Chem. Phys.* **1982**, *77*, 3654−3665.
(73) Tomasi, J.; Mennucci, B.; Cammi, R. *Chem. Rev.* **2005**, *105*, 2999−3093.
(74) Scalmani, G.; Frisch, M. J.; Mennucci, B.; Tomasi, J.; Cammi, R.; Barone, V. *J. Chem. Phys.* **2006**, *124*, 94107.
(75) Takács, A.; Szilágyi, A.; Ács, P.; Márk, L.; Peixoto, A. F.; Pereira, M. M.; Kollár, L. *Tetrahedron* **2011**, *67*, 2402−2406.
(76) Sullivan, B. P.; Salmon, D. J.; Meyer, T. J. *Inorg. Chem.* **1978**, *17*, 3334−3341.

dx.doi.org/10.1021/ic5002623 | *Inorg. Chem.* 2014, 53, 5556−5567